

Melting of iron determined by X-ray absorption spectroscopy to 100 GPa

Giuliana Aquilanti^{a,1}, Angela Trapananti^b, Amol Karandikar^{c,d}, Innokenty Kantor^e, Carlo Marini^{e,2}, Olivier Mathon^e, Sakura Pascarelli^e, and Reinhard Boehler^c

^aElettra-Sincrotrone Trieste, 34149 Basovizza, Trieste, Italy; ^bOperative Group Grenoble (OGG)-Istituto Officina dei Materiali-Consiglio Nazionale delle Ricerche (CNR), 38043 Grenoble Cedex 9, France; ^cGeophysical Laboratory, Carnegie Institution of Washington, Washington, DC 20015; ^dGeowissenschaften, Goethe-Universität, D-60438 Frankfurt a.M., Germany; and ^eEuropean Synchrotron Radiation Facility, 38043 Grenoble Cedex 9, France

Edited by Erio Tosatti, International School for Advanced Studies, Trieste, Italy, and approved August 17, 2015 (received for review February 4, 2015)

Temperature, thermal history, and dynamics of Earth rely critically on the knowledge of the melting temperature of iron at the pressure conditions of the inner core boundary (ICB) where the geotherm crosses the melting curve. The literature on this subject is overwhelming, and no consensus has been reached, with a very large disagreement of the order of 2,000 K for the ICB temperature. Here we report new data on the melting temperature of iron in a laser-heated diamond anvil cell to 103 GPa obtained by X-ray absorption spectroscopy, a technique rarely used at such conditions. The modifications of the onset of the absorption spectra are used as a reliable melting criterion regardless of the solid phase from which the solid to liquid transition takes place. Our results show a melting temperature of iron in agreement with most previous studies up to 100 GPa, namely of 3,090 K at 103 GPa.

iron melting curve | XAS | megabar range

Iron is the principal constituent of the Earth's core (1), and knowledge of its melting curve at inner core boundary (ICB) conditions is one of the major concerns in geophysics. At the ICB, corresponding to a depth of 5,150 km and to a pressure of 330 GPa, the solid inner core melts and the outer core is liquid. Even though the temperature at which the solid core becomes liquid should be adjusted to take into account the effects of light elements in the solid and liquid cores, the knowledge of the melting temperature of iron is an important fixed point in the thermal profile of Earth's interior. Earth's magnetic field is generated by a dynamo in the liquid iron core that has a convection motion as a result of cooling of the overlying mantle. Because the melting temperature of iron puts a constraint on the thermal gradient across the core–mantle boundary and the heat flow from the core, it represents the key to understand Earth's dynamo and therefore the implications to the terrestrial magnetic field.

A considerable effort has been expended to study the melting of iron at high pressure both theoretically (2–5) and experimentally, but this has led to considerable discrepancies in the estimates of the temperature in the center of Earth. This discrepancy, as large as 2,000 K at ICB conditions (330 GPa), has a significant impact on dynamic and thermal evolution models. The numerous studies have been summarized in several recent papers (6, 7).

Besides shock compression, laser heating in diamond anvil cells (LHDAC) allows one to generate the very high pressure and temperature conditions of Earth's core. In LHDAC studies, the maximum pressure for which iron melting temperatures have been reported is 200 GPa (8, 9), but the difference in the melting temperature in these measurements exceeds 1,000 K. Even the two most recent studies using synchrotron X-ray diffraction (XRD) and X-ray Mössbauer techniques (8, 10) show melting temperatures differing by 800 K at 100 GPa. The difficulty in measuring the melting temperature is particularly concerning, given that two X-ray diffraction measurements, carried out at the same beamline at the European Synchrotron Radiation Facility (ESRF) (8, 11), led to a difference in the melting temperature of 980 K at 130 GPa.

Here we report a determination of the solid–liquid phase boundary of iron compressed to over 100 GPa in an LHDAC by means of energy-dispersive X-ray absorption spectroscopy (EDXAS) using a well calibrated optical system and a novel sample encapsulating technique, which avoids chemical reactions and deterioration of the sample geometry.

X-ray absorption spectroscopy (XAS) provides structural information within a few angstroms around the photoabsorbing atom, and therefore maintains the same sensitivity and accuracy regardless of the physical state of the investigated sample (crystalline, amorphous, or liquid). This is a considerable asset with respect to diffraction techniques in which the onset of melting appears as a weak diffuse halo superimposed onto strong Bragg reflections from partially molten sample and sample environment. Similarly to diffraction techniques, X-ray absorption near edge structure (XANES) spectra may distinguish different crystallographic phases, but, in addition, it may shed some light on the electronic structure. A further advantage with respect to other methods is that, given its chemical selectivity, the XANES spectra contain solely the signal relative to the absorbing element, without any interference of the container or experimental environment. This is particularly convenient when the sample environment is particularly bulky, such as at high-pressure conditions. From the XANES part of the spectrum, it is possible to retrieve the coordination geometry of the atom of interest and its speciation, giving information about possible chemical reactions that may

Significance

There is a long-standing controversy over the melting curve of Fe at high pressure as determined from static laser heated diamond anvil cell and dynamic compression studies. X-ray absorption spectroscopy measurements are used here as a criterion to detect melting under pressure. Confronted with a diversity of obtained melting curves, this technique, used at such pressure and temperature conditions, is eligible to be at the forefront to probe Earth's deep interior. Furthermore, the experiment reported here holds promise for addressing important issues related to the structure and phase diagram of compressed melts, such as the existence of structural complexity (polyamorphism) in the liquid phase or the extent of icosahedral ordering whose investigation has been limited until now to ambient conditions.

Author contributions: G.A., A.T., and R.B. designed research; G.A., A.T., I.K., C.M., S.P., and R.B. performed research; G.A., A.T., A.K., I.K., C.M., O.M., S.P., and R.B. contributed new reagents/analytic tools; G.A., A.T., I.K., C.M., and S.P. analyzed data; and G.A., A.T., I.K., and R.B. wrote the paper.

The authors declare no conflict of interest.

This article is a PNAS Direct Submission.

Freely available online through the PNAS open access option.

¹To whom correspondence should be addressed. Email: giuliana.aquilanti@elettra.eu.

²Present address: ALBA Synchrotron, 08290 Cerdanyola del Vallès, Barcelona, Spain.

This article contains supporting information online at www.pnas.org/lookup/suppl/doi:10.1073/pnas.1502363112/-DCSupplemental.

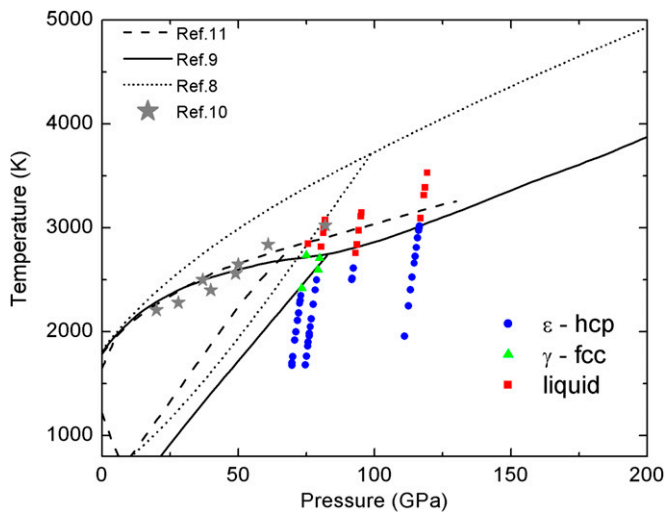


Fig. 3. P–T conditions at which XANES spectra were collected. Blue dots correspond to ϵ -hcp Fe. Green triangles correspond to γ -fcc Fe. Red squares correspond to liquid Fe. Half thermal pressure has been considered. This has been determined from Fe phonon density of states to 151 GPa (10). Phase boundaries for iron from other experimental studies are also shown (solid black line, ref. 9; dashed black line, ref. 11; dotted line, ref. 8; stars, ref. 10).

absorption onset in the liquid phase can therefore be attributed to a broader distribution of empty $4p$ states as a consequence of the lack of crystalline order. The same effect of discontinuous broadening in the XANES spectra has not only been theoretically predicted by DFT calculations on iron at high temperature and pressure conditions (16) but has also been observed experimentally at the solid to liquid transition in other transition metals such as Cu (18) and Ni (19) at ambient pressure. In these studies, the solid to liquid phase transition was additionally confirmed by combined X-ray diffraction measurements.

Fig. 3 shows the P–T conditions at which all of the XANES measurements have been collected. Different symbols and colors correspond to ϵ -Fe (blue dots), γ -Fe (green triangles) and liquid Fe (red squares) phases as determined from the XANES spectra. Phase boundaries reported in refs. 8–11 are also shown for comparison. The phase diagram is reported with thermal pressure corrections (10).

Discussion

In the context of continuous efforts to provide additional experimental data toward resolving the discrepancy in the measured melting curve of Fe at high pressure, the results here reported are an independent measurement of the melting curve obtained by an experimental technique different from those used in previous experimental studies. The XAS experiment provides continuous monitoring of the changes of both the atomic and electronic structure as a function of temperature, and it is optimally suited to detect the onset of order–disorder or solid–liquid transitions. The melting criterion here adopted is based on changes occurring in the near-edge region of the absorption spectrum (XANES) that is known to be less affected by thermal damping and by the noise associated with extreme experimental conditions. We show here that the detection of the new phase does not appear gradually as a weak background superimposed to a much larger signal as in XRD methods but as a discontinuous change in the XANES signal that has similar amplitude with respect to that in the solid phase. This is an advantage of XANES over XRD because, in a partially molten sample caused by temperature instabilities (11), the signature of the melting has the same intensity as that of the solid sample whereas, in XRD,

the diffused halo characteristic of the liquid sample is weak with respect to the signal coming from the solid part of the sample. This is especially true when phenomena defined as “recrystallization” (11) or “fast crystallization” (8) occur, giving rise to intense Bragg peaks.

Fig. 4 reports a comparison between the experimental XANES recorded at 68 GPa at different temperatures (blue line, ϵ -Fe (hcp); green line, γ -Fe (fcc); red line, liquid iron) compared with full multiple-scattering calculations to simulate the XANES region of the spectra at thermodynamic conditions comparable to the experimental ones (the details of the calculations are reported in *Supporting Information*). Concerning the hcp to fcc transition, the calculations confirm the flattening of the bump “b” and the shifts of the maximum “c” to lower energy. On the other side, the XANES calculation of iron in the fcc phase shows a second maximum just above 7,135 eV which is less evident in the experimental data presented in this work. As well, the smoothing of the plateau “a” discussed before on Fig. 1 is less pronounced in the calculated XANES. Approximations used for the theoretical XANES calculations could be invoked to explain these discrepancies. More interesting, instead, is the behavior of the onset of the absorption that has been used in discussing Fig. 2 as a signature for the solid to liquid phase transition. In fact, consistent with the experimental

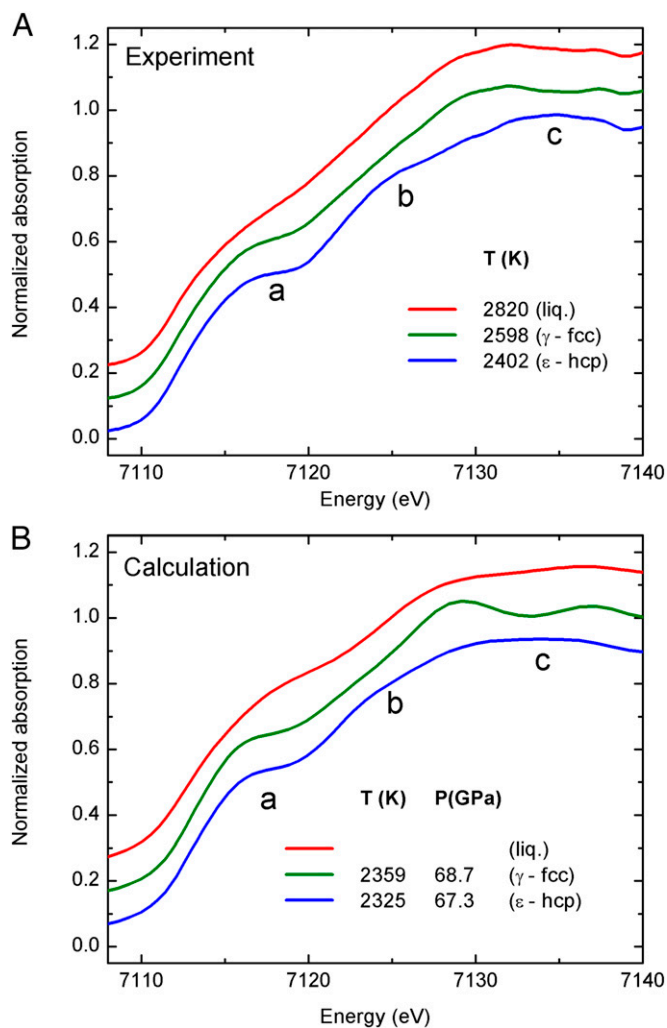


Fig. 4. Experimental XANES spectra of iron recorded at 68 GPa (A). Calculated XANES spectra of iron in the ϵ -hcp phase (blue line), γ -fcc phase (green line), and liquid phase (red line) (B).

data, the XANES calculation shows the same modifications of plateau “a” between 7,115 eV and 7,120 eV in the liquid phase with respect to the solid phases characteristic of the disruption of the crystalline order.

The present results show excellent agreement for the ϵ -Fe (hcp) to γ -Fe (fcc) transition reported earlier (6, 7), and the present melting data are in agreement with most previous studies up to 100 GPa resulting in a flat melting curve near 3,000 K at that pressure range. This is in stark disagreement with the recent XRD study by Anzellini et al. (8). The latter reports a much steeper melting curve at that pressure range and a melting temperature that is 700 K higher than the majority of all previous studies (6). This difference has significant implications for estimating the temperature in Earth’s interior, which determines the value of the temperature jump at the core–mantle boundary, which is key for calculating the core–mantle heat flow, inner core age, dynamo models, and cooling history of Earth. Although an accurate extrapolation of the present data to Earth’s core conditions is difficult given the limited number of experimental data above the triple point, our results are in agreement with the majority of diamond anvil cells (DACs) measurements in the 100-GPa pressure range (7) and with previous data to 200 GPa (9). The latter suggests a melting temperature of iron below 5,000 K when extrapolated to ICB conditions.

The experimental method here reported paves the way for extensive studies of molten metals at extreme pressures. For liquids, it is known that frustration, defined as the presence of locally preferred structures incompatible with the crystal periodicity, may have important consequences in the melting. For molten iron, together with other metals with partially filled d bands, liquid frustration was proposed as an explanation for the low slope of the melting curve (20). In the present work, the analysis is focused on the features of the near-edge region of the XAS spectrum because they are clear fingerprints for the occurrence of melting. However, previous studies have demonstrated that XAS is capable to evidence the existence and extent of preferred local geometries in molten metals at ambient conditions (18, 19). Therefore, beyond geophysical implications, the present results may be used to investigate the structure of compressed liquid Fe and possibly validate the hypothesis on the presence of frustration.

Materials and Methods

The pressure is generated using a Boehler–Almax plate DAC equipped with monocrystalline conical diamond anvils (21) of 250–300 μm of diameter. A rhenium gasket is preindented to a thickness 40 μm . A hole of 100 μm diameter is then drilled on the culet imprint.

The sample container consists of two discs of sapphire manufactured using a combination of micropolishing and focused ion beam milling (FIBM). The cavity dimension of 18 μm diameter and 6 μm depth is chosen to optimize the synchrotron beam condition at the beamline ID24 (22) at ESRF. The single-crystal capsule and its lid are embedded in very fine-grained (3–5 μm grain size) dried Al_2O_3 powder, which molds around the capsule to prevent fracture during loading and after laser heating. One ruby grain of 2–3 μm size was also mixed with the Al_2O_3 powder (see [Supporting Information](#)).

The principal optical layout of the laser heating and temperature measurement system is very similar to the one described in ref. 23. The major difference is that the optical components do not interfere with the direct X-ray beam, allowing true simultaneous measurements of temperature from both sides of the sample as well as the X-ray absorption spectra. Further details are given in [Supporting Information](#).

The XAS measurements in transmission geometry are carried out at the dispersive extended X-ray absorption fine structure (EXAFS) beamline ID24 at ESRF (22). The size of the beam at the sample is of $5 \times 5 \mu\text{m}^2$ FWHM. Spectra are recorded using a CCD-based position sensitive detector. Pixel energy calibration is obtained by measuring spectra on a metallic Fe foil at ambient conditions. XAS spectra are collected every few seconds before, during, and after heating in four different runs in the pressure range 63–103 GPa and temperatures up to 3,530 K. For each heating cycle, the laser power is ramped up incrementally and kept constant for several seconds to record the XAS spectrum and light emission to measure the temperature. Pressures are determined before and after heating cycles using both ruby and the Raman spectra of the diamond anvil tips (24), with the accuracy within 2 GPa at the highest pressure achieved. After several heating cycles, these pressures are within 5 GPa. XANES spectra of the same sample are recorded at the beginning of each heating cycle and show that chemical reactions of the sample with the environment, if any, occur for a fraction of the sample that is below the XANES detection limit. Moreover, in each cycle we find the same transition temperatures within the experimental error. See [Supporting Information](#) for additional experimental details.

ACKNOWLEDGMENTS. The authors acknowledge the European Synchrotron Radiation Facility for provision of beam time. G.A. and R.B. acknowledge the European Synchrotron Radiation Facility for financial support during in-house experiments. A.K. and R.B. acknowledge funding from National Science Foundation Grant EAR 1248553.

- Poirier J-P (2000) *Introduction to the Physics of the Earth’s Interior* (Cambridge Univ Press, New York), 2nd Ed.
- Alfè D, Gillan MJ, Price GD (1999) The melting curve of iron at the pressures of the Earth’s core from ab initio calculations. *Nature* 401(6752):462–464.
- Laio A, Bernard S, Chiarotti GL, Scandolo S, Tosatti E (2000) Physics of iron at Earth’s core conditions. *Science* 287(5455):1027–1030.
- Sola E, Alfè D (2009) Melting of iron under Earth’s core conditions from diffusion Monte Carlo free energy calculations. *Phys Rev Lett* 103(7):078501.
- Belonoshko AB, Ahuja R, Johansson B (2000) Quasi-ab initio molecular dynamic study of Fe melting. *Phys Rev Lett* 84(16):3638–3641.
- Komabayashi T, Fei Y (2010) Internally consistent thermodynamic database for iron to the Earth’s core conditions. *J Geophys Res* 115(B3):B03202.
- Boehler R, Ross M (2007) Properties of rocks and minerals – High-pressure melting. *Treatise on Geophysics*, ed Schubert G (Elsevier, Amsterdam), pp 527–541.
- Anzellini S, Dewaele A, Mezouar M, Loubeyre P, Morard G (2013) Melting of iron at Earth’s inner core boundary based on fast X-ray diffraction. *Science* 340(6131):464–466.
- Boehler R (1993) Temperatures in the Earth’s core from melting-point measurements of iron at high static pressures. *Nature* 363(6429):534–536.
- Jackson JM, et al. (2013) Melting of compressed iron by monitoring atomic dynamics. *Earth Planet Sci Lett* 362:143–150.
- Boehler R, Santamaría-Pérez D, Errandonea D, Mezouar M (2008) Melting, density, and anisotropy of iron at core conditions: New X-ray measurements to 150 GPa. *J Phys Conf Ser* 121(2):022018.
- Boehler R, Musshoff HG, Ditz R, Aquilanti G, Trapananti A (2009) Portable laser-heating stand for synchrotron applications. *Rev Sci Instrum* 80(4):045103.
- Mathon O, et al. (2004) Dynamics of the magnetic and structural α - ϵ phase transition in iron. *Phys Rev Lett* 93(25):255503.
- Filippini A, et al. (1998) Single-energy X-ray absorption detection: A combined electronic and structural local probe for phase transitions in condensed matter. *J Phys Condens Matter* 10(11):235.
- Marini C, et al. (2014) A microsecond time resolved X-ray absorption near edge structure synchrotron study of phase transitions in Fe undergoing ramp heating at high pressure. *J Appl Phys* 115(9):093513.
- Mazevet S, et al. (2014) Ab initio calculation of x-ray absorption of iron up to 3 Mbar and 8000 K. *Phys Rev B* 89(10):100103.
- Raji AT, Scandolo S, Härting M, Britton DT (2013) Probing the structure of iron at extreme conditions by X-ray absorption near-edge structure calculations. *High Pressure Res* 33(1):119–123.
- Di Cicco A, Trapananti A (2007) Study of local icosahedral ordering in liquid and undercooled liquid copper. *J Non-Cryst Solids* 353(32-40):3671–3678.
- Di Cicco A, et al. (2014) Local fivefold symmetry in liquid and undercooled Ni probed by x-ray absorption spectroscopy and computer simulations. *Phys Rev B* 89(6):060102.
- Ross M, Boehler R, Errandonea D (2007) Melting of transition metals at high pressure and the influence of liquid frustration: The late metals Cu, Ni, and Fe. *Phys Rev B* 76(18):184117.
- Boehler R, De Hantsetters K (2004) New anvil designs in diamond-cells. *High Pressure Res* 24(3):391–396.
- Pascarelli S, Mathon O, Muñoz M, Mairs T, Susini J (2006) Energy-dispersive absorption spectroscopy for hard-X-ray micro-XAS applications. *J Synchrotron Radiat* 13(Pt 5):351–358.
- Boehler R (2000) High-pressure experiments and the phase diagram of lower mantle and core materials. *Rev Geophys* 38(2):221–245.
- Akahama Y, Kawamura H (2010) Pressure calibration of diamond anvil Raman gauge to 410 GPa. *J Phys Conf Ser* 215(1):012195.
- Murphy CA, Jackson JM, Sturhahn W, Chen B (2011) Melting and thermal pressure of hcp-Fe from the phonon density of states. *Phys Earth Planet Inter* 188(1-2):114–120.
- Ravel B, Newville M (2005) ATHENA, ARTEMIS, HEPHAESTUS: Data analysis for X-ray absorption spectroscopy using IFEFFIT. *J Synchrotron Radiat* 12(Pt 4):537–541.
- Rehr JJ, Kas JJ, Vila FD, Prange MP, Jorissen K (2010) Parameter-free calculations of X-ray spectra with FEFF9. *Phys Chem Chem Phys* 12(21):5503–5513.
- Komabayashi T, Fei Y, Meng Y, Prakapenka V (2009) In-situ X-ray diffraction measurements of the γ - ϵ transition boundary of iron in an internally-heated diamond anvil cell. *Earth Planet Sci Lett* 282(1-4):252–257.
- Soper AK (1996) Empirical potential Monte Carlo simulation of fluid structure. *Chem Phys* 202(2-3):295–306.
- Waseda Y (1980) *The Structure of Non-Crystalline Materials* (McGraw-Hill, New York).